



# Electrochemical water oxidation on WO<sub>3</sub> surfaces: A density functional theory study



Ravi Kishore<sup>a,1</sup>, Xi Cao<sup>b,1</sup>, Xueqing Zhang<sup>a,c,\*</sup>, Anja Bieberle-Hütter<sup>a,c,\*</sup>

<sup>a</sup> *Electrochemical Materials and Interfaces, Dutch Institute for Fundamental Energy Research (DIFFER), De Zaale 20, 5612AJ, Eindhoven, The Netherlands*

<sup>b</sup> *Center for Computational Energy Research, Department of Applied Physics, Eindhoven University of Technology, P.O. Box 513, 5600MB, Eindhoven, The Netherlands*

<sup>c</sup> *Center for Computational Energy Research, Dutch Institute for Fundamental Energy Research (DIFFER), De Zaale 20, 5612AJ, Eindhoven, The Netherlands*

## ARTICLE INFO

### Keywords:

Density functional theory  
Oxygen evolution reaction  
Tungsten oxide  
Overpotential  
Doping

## ABSTRACT

Density functional theory (DFT) calculations are performed to study the oxygen evolution reaction (OER) on tungsten oxide (WO<sub>3</sub>) surfaces. The free energies of the proton coupled electron transfer (PCET) steps are calculated and from these the OER overpotential is calculated as the characteristic parameter for the electrochemical activity. The effects of surface orientation, oxygen vacancies, and doping by Chromium (Cr) and Molybdenum (Mo), on the OER activities are analyzed. The difference in OER overpotential for the three surface orientations, (200), (002) and (020), is found to be very small (0.07 V). The presence of oxygen vacancies in the first WO<sub>3</sub> sub-layer do not favor OER, while vacancies in the second sub-layer do reduce the OER overpotential. A volcano plot with all overpotentials calculated in this study shows that the OER is favored at the Mo doped (200) surface (reactions happen at the Mo site). This paper demonstrates that DFT calculations of the electrochemical activity are an efficient method to identify active surfaces and can therefore save a lot of experimental effort in designing more efficient photoelectrodes for water splitting.

## 1. Introduction

Energy storage is one of the biggest challenges facing the growth of renewable energy, especially wind and solar energy. Storage in the form of solar fuels like hydrogen is a promising solution [1–9]. Hydrogen can be produced by splitting of water by two routes, by the indirect route where electricity from a photovoltaic (PV) generator can be transferred to an electrolyser by the direct photoelectrochemical (PEC) route where hydrogen is generated at the surface of a photoactive semiconductor immersed in an electrolyte [10]. The latter route has clear advantages related to integration, but efficiency still needs to be increased [10].

The photoelectrodes in PEC water splitting cells are made of semiconductor materials. Electrons are excited with the help of light from their ground state (valence band, VB) to the excited state (conduction band, CB) leaving a positively charged hole in the VB. Hence, an electron–hole pair is created. In an n-type semiconductor, the electrons travel to the counter electrode where they reduce water and hydrogen is formed ( $4\text{H}_2\text{O} + 4\text{e}^- \rightarrow 4\text{OH}^- + 2\text{H}_2$ ). This is called the hydrogen evolution reaction (HER). The holes migrate to the surface of the photoelectrode, where they oxidize water to form oxygen ( $4\text{OH}^- + 4\text{H}^+ \rightarrow 2\text{H}_2\text{O} + \text{O}_2$ ). This is called the oxygen evolution reaction

(OER). We focus in this paper on the OER because it accounts for most of the overpotential required to drive water splitting [3,11,12].

The first demonstration of PEC water splitting was given by Fujishima et al. [13] on the surface of Titanium Oxide (TiO<sub>2</sub>). Metal oxides are found to be stable in photoelectrochemical environment with a reasonable band gap. Hence, they often attract interests for PEC water splitting. Lots of oxide materials have been proposed for PEC application. However, each material has its own disadvantage. Tungsten oxide (WO<sub>3</sub>) is an interesting material because of its photoelectrochemical stability for pH < = 4, a suitable band gap (2.4–2.8 eV [14]) which favors visible light absorption [15,16]. It is also non-toxic and can be prepared in high purity [17]. In their experimental studies, He et al. [18] have found enhancement of photo-catalytic activity in WO<sub>3</sub> when coupled with Sb<sub>2</sub>O<sub>3</sub> through the photo-catalytic degradation of aqueous Rh mixed with different WO<sub>3</sub>/Sb<sub>2</sub>O<sub>3</sub> samples. Ng et al. [19] demonstrated band gap reduction from 2.74 eV to 2.60 eV experimentally and increased of photo-activity of WO<sub>3</sub> when the anode was doped with 20% Ga. Wang et al. [14] used Mo and Cr as dopants, replacing W atoms in the lattice, which narrows the band gap. Doping with lower valence elements like Ti, Zr and Hf was also investigated [14]. The band gap position and value were found to improve in these cases. It has been

\* Corresponding authors.

E-mail addresses: [X.Zhang@diffier.nl](mailto:X.Zhang@diffier.nl) (X. Zhang), [A.Bieberle@diffier.nl](mailto:A.Bieberle@diffier.nl) (A. Bieberle-Hütter).

<sup>1</sup> These authors contributed equally to this work.

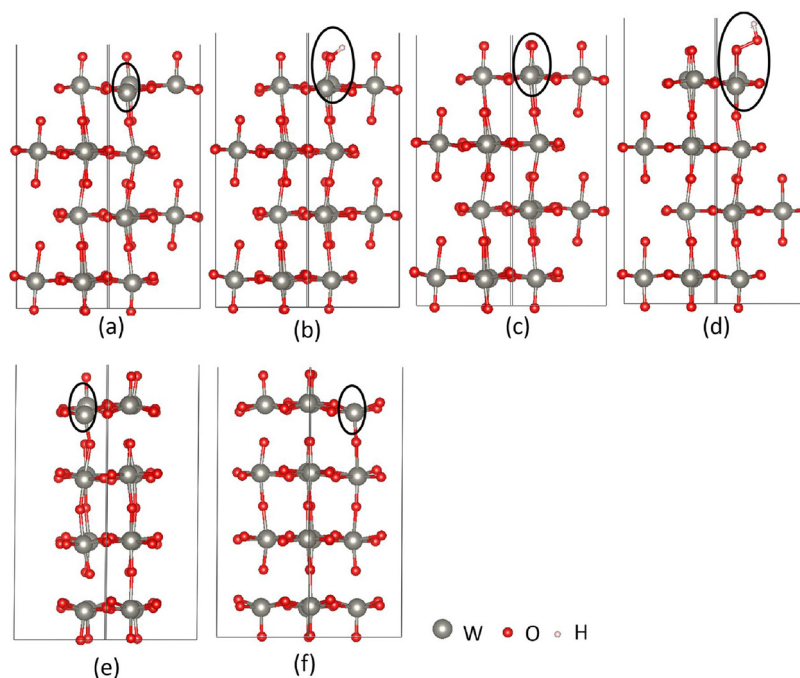


Fig. 1. The relaxed  $\text{WO}_3$  (200) geometry with (a) free site (b) OH (c) O (d) OOH adsorbed on the surface, (e) the relaxed  $\text{WO}_3$  (002) geometry with free site, (f) the relaxed  $\text{WO}_3$  (020) geometry with free site.

reported experimentally that Mo doping leads to a favourable band gap for water oxidation [20]. Mo-doped  $\text{WO}_3$  nanowires ( $\text{Mo}_x\text{W}_{1-x}\text{O}_3 \cdot 0.33\text{H}_2\text{O}$ ) showed that the band gap of the solid solutions was narrowed by 0.48 eV with Mo content increasing from  $x = 0$  to  $x = 0.75$  [20]. However, the catalytic roles of the doping elements are not known from these experimental studies. The effects of doping with Ti, Mn, Co, Ni, and Pt on the OER overpotential have been investigated theoretically by Liao et al. [21] and Neufeld et al. [22] Co and Ni were predicted as effective dopants for electrocatalysis of water with hematite [21]. Based on surface electronic structure calculations, García-Mota et al. discussed how one can tailor the surface reactivity of  $\text{TiO}_2$  by transition-metal substitution [7]. The oxygen-surface interaction is related to the presence of the surface states and the surface resonance states.

Despite the importance of tungsten oxide in various areas of catalysis and photo-electrocatalysis, relatively few theoretical studies have been devoted to this system. The theoretical studies have been focused merely on electronic structure calculations [23–25]. The reader is referred to the review by Valentin et al. [26].

Valdes et al. [27] have studied the oxidation of water on tungsten trioxide by first principles simulations. The authors analyzed the overpotential needed for the photoelectrolysis of water and found that the limiting step is the deprotonation of surface adsorbed OH. Various studies report the improvement in performance of hematite photoanodes in the presence of oxygen vacancies [28–30]. In this study we perform DFT calculations of OER on  $\text{WO}_3$  surfaces with oxygen vacancies in the sub-layers below the top surface.

The aim of the present work is the calculation of the overpotential of the oxygen evolution on  $\text{WO}_3$  surfaces in various geometries, including different surface orientations, the impact of doping elements, and oxygen vacancies.

## 2. Model and methods

Many reaction mechanisms on the OER on metal oxide surfaces were proposed in the literature as discussed in a recent review paper by Zhang and Bieberle-Hütter [3]. Here we consider the mechanism proposed by Rossmesl et al. [31] This mechanism has been used in many

studies [32–36]. The OER mechanism is considered to proceed in the following four steps:



The free energy ( $\Delta G$ ) for each step is calculated following the approach discussed in Ref. [31] The maximum step of these four steps is the potential determining step. The entire process has an energy change of 4.92 eV (i.e. 1.23 eV for each PCET step). The DFT calculations are carried out using Vienna ab initio simulation package (VASP) developed by Fakultät für Physik of the Universität Wien [37–40]. The plane wave energy cutoff of 700 eV was used in the calculations. The Perdew–Burke–Ernzerhof (PBE) XC functional [41] and the projected augmented wave (PAW) [42,43] potentials were used. The importance of considering solvation effects on OER intermediates was shown by Gauthier et al. [8] and Dickens et al. [44] While important, optimizing explicit solvation structures for each surface considered here comes with exceptional computational cost. Thus, we have limited the scope of this study to compare the OER activities with a solid-gas model. The corrections, including dipole, Hubbard U, and implicit solvation were found to have small effects on the free energy steps as shown in Fig. S2. Therefore these effects are not discussed in the main text. More computational details are given in the supporting information.

The bulk monoclinic  $\text{WO}_3$  geometry and cell parameters are optimized by DFT. The required surfaces are then cleaved based on the optimized bulk geometry. These surface structures are again optimized for a minimum energy. In Fig. 1, we show the relaxed geometries exemplarily for different adsorption sites, namely free surface site, OH, O, and OOH adsorbed (Fig. 1a–d) and different surface orientations, i.e. (200), (002), and (020) (Fig. 1(a, e, f)).

The reaction free energies under an applied potential  $U$  can be calculated as follows.

$$\Delta G_1 = E(*\text{OH}) - E(*) - E_{\text{H}_2\text{O}} + \frac{1}{2}E_{\text{H}_2} + (\Delta ZPE - T\Delta S)_1 - eU \quad (5)$$

$$\Delta G_2 = E(*O) - E(*OH) + \frac{1}{2}E_{H_2} + (\Delta ZPE - T\Delta S)_2 - eU \quad (6)$$

$$\Delta G_3 = E(*OOH) - E(*O) - E_{H_2O} + \frac{1}{2}E_{H_2} + (\Delta ZPE - T\Delta S)_3 - eU \quad (7)$$

$$\Delta G_4 = E(*) - E(*OOH) + E_{O_2} + \frac{1}{2}E_{H_2} + (\Delta ZPE - T\Delta S)_4 - eU \quad (8)$$

$\Delta G_n$  are the free energy steps.  $\Delta ZPE$  is the difference in zero point energies due to the reaction,  $\Delta S$  is the change in entropy. The overpotential which is used as the determining parameter for the electrochemical activity, is defined as:

$$\eta = \max(\Delta G_1, \Delta G_2, \Delta G_3, \Delta G_4) - 1.23eV \quad (9)$$

The surface geometry with the minimum value of overpotential is the most efficient with regard to oxygen evolution. By comparing the calculated overpotentials for different surfaces, we can identify the most efficient  $WO_3$  surface for OER from the systems under consideration.

### 3. Results and discussion

We have studied the effect of surface orientation, doping, and oxygen vacancies on the oxygen evolution reaction. In this section we discuss these effects on the OER activities based on the free energy step calculations.

#### 3.1. Surface orientation

The surface orientation has been reported to be a sensitive parameter that affects the OER overpotential for  $RuO_2$  [45] and hematite systems [34]. To study orientation sensitivity of OER on  $WO_3$  surface, we choose the (200), (020), and (002) orientations as these surfaces showed high PEC activity experimentally [46]. We performed free energy calculations for each PCET step of the OER on these surfaces.

Fig. 2 compares the free energies versus the four reaction steps for the (200), (020) and (002) surfaces. The overpotential is calculated based on Eq. (9). Compared to the (200) surface, both OH and O are destabilized on (002) and (020), respectively. However, the potential determining step, i.e. the overpotential, is lower for (002) and (020). The potential determining step is  $\Delta G_2$  for the (200) and (020) surface, while  $\Delta G_1$  is the potential determining step for the (002) surface. The difference in overpotential for the three orientations in general is very small with only 0.07 eV. We can therefore conclude that the orientation has negligible effect on the catalytic properties for OER at these surfaces. This is in good agreement with the finding of Valdes et al. [47]. The authors found an overpotential of 1.04 eV, 1.10 V and 1.05 V for the (200), (020) and (002) surfaces respectively. The difference in overpotential for the three orientations was 0.06 eV. The potential determining step was the deprotonation of surface adsorbed OH ( $\Delta G_2$ ) for the three orientations in their study. We find that  $\Delta G_2$  is the potential determining step for (020) and (200) surfaces, while  $\Delta G_1$  is found to be potential determining for the (002) surface.

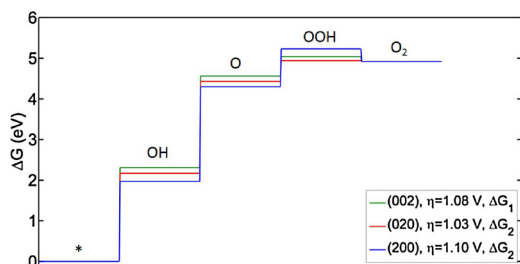


Fig. 2. Free energy versus reaction step of the OER for different orientations of  $WO_3$ : (200), (020) and (002)  $\Delta G_n$  indicates the potential determining step.

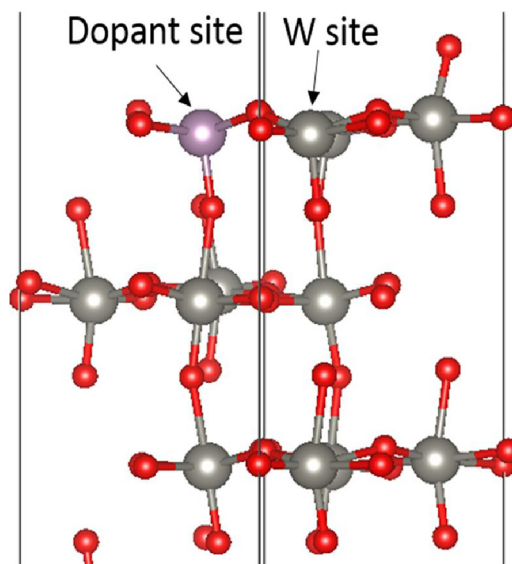


Fig. 3. Schematic geometry of  $WO_3$  (200) with one W atom on the top surface being replaced by a dopant atom. The two reaction sites calculated in this study are indicated by arrows: reaction on dopant site and reaction on W site.

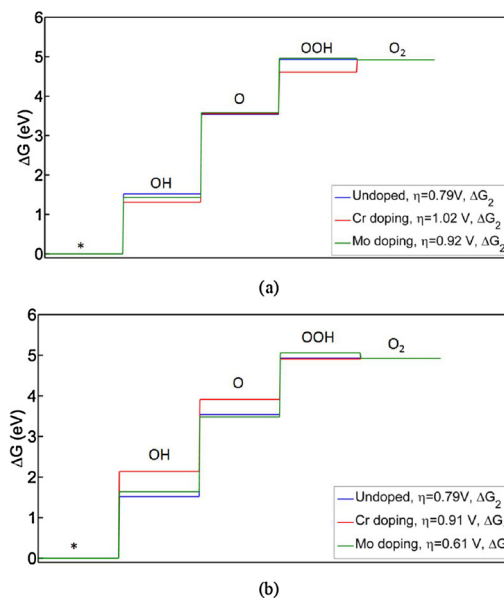
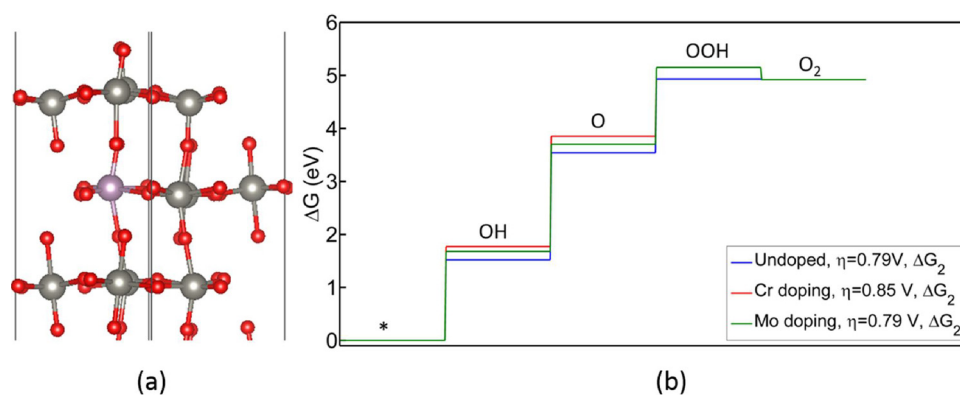


Fig. 4. Free energy versus reaction step of the OER for pure and doped (200)  $WO_3$  (with the dopants at the first layer, Fig. 3) with reaction occurring on (a) the W atom and (b) the dopant atom.

#### 3.2. Doping

The effects of Mo and Cr doping on the band gap of  $WO_3$  have been discussed in the literature [14,20]. In this work, we study the effects of Cr and Mo doping on the OER activities on (200) surface by substituting a W atom by the dopant atom in the first and the second layer of the geometry. We investigate two reaction sites: a) the reaction occurs on a W site (at the neighbor of the dopant atom) and b) the reaction occurs on the dopant site (Fig. 3). The effects of the termination and coverage on the OER activities have been discussed by García-Mota et al. [6] and Diaz-Morales et al. [5] for the Co and Ni systems respectively. Fig. S4 shows the effects of different surface coverages (O covered vs. half O covered) and different terminations (O covered vs. OH covered) on the OER free energy steps. It is found that the surface with half coverage of O is the most active as shown in Fig. S4. Therefore, we choose the half-



**Fig. 5.** (a) Schematic geometry of WO<sub>3</sub> (200) with one W atom at the second layer being replaced by a dopant atom. (b) Free energy versus reaction step of the OER for undoped and doped (200) WO<sub>3</sub> with the dopants at the second layer.

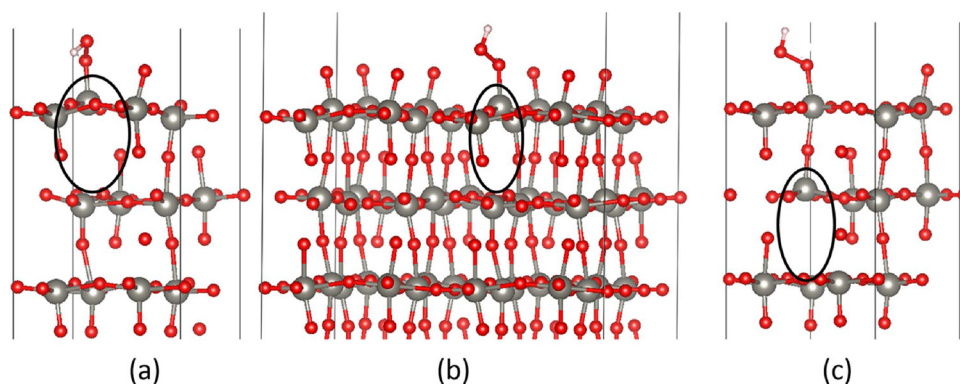


**Fig. 6.** Relaxed oxygen vacancy configurations for WO<sub>3</sub> (200) surface. (a) Oxygen vacancy concentration 1.67/nm<sup>2</sup> in the first layer below the reaction site, (b) Oxygen vacancy concentration 0.41/nm<sup>2</sup> with four times increase in simulation cell, (c) Oxygen vacancy concentration 1.67/nm<sup>2</sup>, located two layers below the reaction site.

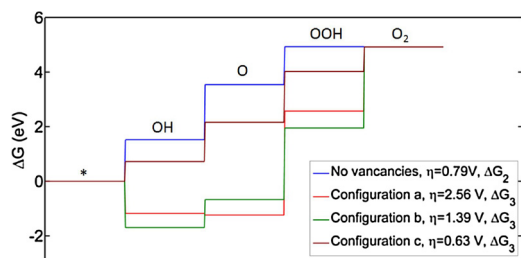


**Fig. 7.** Free energy versus reaction step of the OER for WO<sub>3</sub> (200) surface as a function of oxygen vacancies. The configurations a, b and c refer to Fig. 7(a, b, and c) respectively.

covered O surface for the following free energy calculations.

The comparison of undoped and doped WO<sub>3</sub> with the reactions occurring on the W site shows that for all cases the formation of O is the potential determining step (Fig. 4a). Doping with either Cr or Mo cannot reduce the overpotential (1.02 and 0.92 V, respectively). When

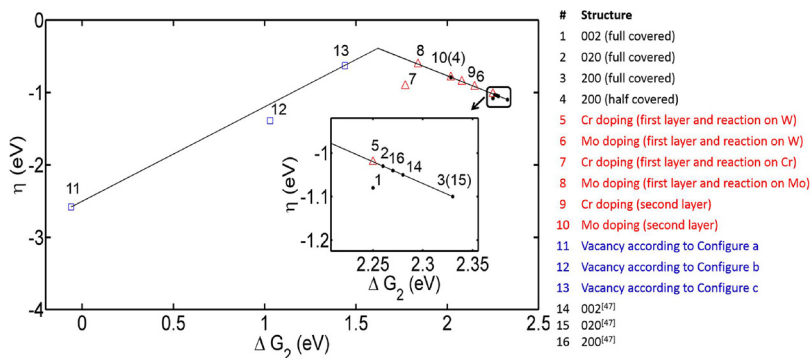


**Fig. 8.** Volcano plot (overpotential vs.  $\Delta G_2$ ) for the oxygen evolution reaction on all WO<sub>3</sub> surfaces investigated in this study. The values from ref. [47] are added for comparison. Half O and full O indicate full and half coverage of O respectively. The volcano lines are added for guiding the eye. The data points are grouped with different colors (red for doping, blue for vacancy, and black for the rest) for clarity. (For interpretation of the references to colour in this figure legend, the reader is referred to the web version of this article.)

in overpotential is very small. For the case of Mo doping, it does not change the OER overpotential. There is an increase of 0.06 eV in the overpotential for the Cr doping at the second layer. Hence, we can summarize that the doping in the second layer has very small effect on the OER activities.

### 3.3. Oxygen vacancies

Zhang et al. [30] carried out DFT calculations of hematite surfaces with different concentrations of oxygen vacancies in the first sublayer. Whereas the OER overpotential for hematite surfaces without vacancy is around 0.8 V, the overpotential decreased to as low as 0.47 V for an oxygen vacancy concentration of 1.26/nm<sup>2</sup> for the hematite (110) surface. To study the effect of oxygen vacancy concentration and position in WO<sub>3</sub>, we have built three configurations (Fig. 6). We first remove an oxygen directly below the reaction site (Fig. 6(a)), resulting in an O vacancy concentration of 1.67/nm<sup>2</sup>. Further we reduce this concentration to 0.41/nm<sup>2</sup> by increasing the surface area four times as shown in Fig. 6(b). In another configuration, we keep the vacancy concentration 1.67/nm<sup>2</sup> but remove the oxygen atom in the second sub-layer below and from a vacancy which is not directly below the reaction site as shown in Fig. 6(c).

Fig. 7 shows the effect of oxygen vacancies on the free energy steps of the OER. For configurations shown in Fig. 6(a and b), overpotentials of 2.56 V and 1.81 V (with the OOH formation as the potential determining step) were found; these are higher than the vacancy free surface (0.79 V). The first step (OH formation) is negative which means that the energy gain due to change in the surface is more than the energy required by the first OER step. The energy of the vacancy slab is less stable (0.01 eV/atom) than the slab without a vacancy. The changes in the W-W atomic distance are shown in Fig. S6. When the OH is absorbed, the W-W distance (the O vacancy is between the two measured W atoms) increased by 0.029 nm, as indicated in Fig. S6 of the supporting information. Thus, it may be concluded that for the (200) surface of WO<sub>3</sub>, OH adsorption results in a change in the local structure. This leads to an unfavorable OER. It was found that the bindings of OH and OOH are related to each other by a constant of approximately 3.2 eV [9] In Fig. S3, the adsorption energy of OOH is plotted against the adsorption energy of OH. The geometries a and b (geometries shown in Fig. 6(a and b)) do not follow the scaling relationship, however, the OER overpotential is very high.

For the configuration shown in Fig. 6(c), i.e. a geometry with oxygen vacancy in the second sub-layer and with the reaction occurring on a tungsten atom which is not directly above the vacancy, the overpotential decreased by 0.16 V with respect to the vacancy free (200) surface. Zhang, et al. [30] found an optimum vacancy concentration to enhance the OER activity for hematite (110) surface while the reaction occurs on the Fe atom above the vacancy. However, our simulations demonstrate that this is not applicable to WO<sub>3</sub>. The adsorbates induced changes in the local geometry leads to a higher overpotential. The presence of oxygen vacancies in WO<sub>3</sub> increases the overpotential for the two concentrations studied. The only case we found to improve the overpotential is that the OER occurs at a different site rather than the W site above the vacancy (with the vacancy in the second sub-layer). For this case, the reaction site is more stable than the first sublayer vacancy.

### 3.4. Volcano plot

The analysis of the OER in form of volcano plots has been previously successfully applied for different oxide systems [9]. Fig. 8 shows the volcano plot for the OER on WO<sub>3</sub> surfaces investigated in this study. The negative value of calculated overpotential is shown. Hence, the top of the volcano shows the best OER activity (the lowest overpotential). The overview of the volcano plot shows that the overpotential depends strongly on oxygen vacancies and doping, while the surface orientation has very small effect. There are two data points on top of the volcano

plot: the Mo doping (first layer and reaction on dopants, data points 8) and the oxygen vacancy according to configuration c (O vacancy concentration 1.67/nm<sup>2</sup>; located two layers below the reaction site) (data point 13). However, the presence of oxygen vacancy (O vacancy concentration 1.67/nm<sup>2</sup>; located one layer below the reaction site) results in the highest overpotential (data point 11) due to the stability issue.

## 4. Conclusions

In this study, we investigated the OER activity of WO<sub>3</sub> surfaces. From DFT calculations of the OER activity of (200), (020) and (002) surfaces, we conclude that the WO<sub>3</sub> surface orientation has negligible effect on the OER overpotential. The OER is most favorable at surfaces with half coverage of O. Mo doping is effective in reducing the overpotential for (200) surface. The doping is found to be more effective when the reaction occurs on the dopant site than when the reaction occurs on the W atom. The second layer doping is found to have negligible effect on OER overpotential. The calculations demonstrate that the presence of oxygen vacancies in the first sub-layer does not decrease the overpotential, whereas the oxygen vacancies in the second sub-layer do. The volcano plot analysis shows that the Mo doping (first layer and reaction on dopants) and the presence of oxygen vacancy (O vacancy concentration 1.67/nm<sup>2</sup>; located two layers below the reaction site) are most efficient towards OER. The DFT calculations demonstrated that modeling of the electrochemical activity is a viable method to design electrochemical surfaces for efficient OER.

## Acknowledgements

Zhang and Bieberle-Hütter acknowledge the financial support from NWO (FOM program nr. 147 “CO2 neutral fuels”) for carrying out this study. Supercomputing facilities of the Dutch national supercomputers SURFsara/Lisa and Cartesius are acknowledged.

## Appendix A. Supplementary data

Supplementary data associated with this article can be found, in the online version, at <https://doi.org/10.1016/j.cattod.2018.02.030>.

## References

- [1] S. Bensaid, G. Centi, E. Garrone, S. Perathoner, G. Saracco, Towards artificial leaves for solar hydrogen and fuels, *ChemSusChem* 5 (2012) 500–521.
- [2] M. Grätzel, Photoelectrochemical cells, *Nature* 414 (2001) 338–344.
- [3] X. Zhang, A. Bieberle, Modeling and simulations in photoelectrochemical water oxidation: from single level to multiscale modeling, *ChemSusChem* 9 (2016) 1223–1242.
- [4] D.G. Nocera, The artificial leaf, *Acc. Chem. Res.* 45 (2012) 767–776.
- [5] O. Diaz-Morales, I. Ledezma-Yanez, M.T.M. Koper, F. Calle-Vallejo, Guidelines for the rational design of Ni-based double hydroxide electrocatalysts for the oxygen evolution reaction, *ACS Catal.* 5 (2015) 5380–5387.
- [6] M. García-Mota, M. Bajdich, V. Viswanathan, A. Vojvodic, A.T. Bell, J.K. Nørskov, Importance of correlation in determining electrocatalytic oxygen evolution activity on cobalt oxides, *J. Phys. Chem. C* 116 (2012) 21077–21082.
- [7] M. García-Mota, A. Vojvodic, F. Abild-Pedersen, J.K. Nørskov, Electronic origin of the surface reactivity of transition-metal-doped TiO<sub>2</sub>(110), *J. Phys. Chem. C* 117 (2013) 460–465.
- [8] J.A. Gauthier, C.F. Dickens, L.D. Chen, A.D. Doyle, J.K. Nørskov, Solvation effects for oxygen evolution reaction catalysis on IrO<sub>2</sub>(110), *J. Phys. Chem. C* 121 (2017) 11455–11463.
- [9] I.C. Man, H.-Y. Su, F. Calle-Vallejo, H.A. Hansen, J.I. Martínez, N.G. Inoglu, J. Kitchin, T.F. Jaramillo, J.K. Nørskov, J. Rossmeisl, Universality in oxygen evolution electrocatalysis on oxide surfaces, *ChemCatChem* 3 (2011) 1159–1165.
- [10] R. van de Krol, M. Grätzel, Benchmark for Photoelectrochemical Water Splitting, *Photoelectrochemical Hydrogen Production*, Springer Science + Business Media, 2012 (pp. 9).
- [11] P. Liao, E.A. Carter, New concepts and modeling strategies to design and evaluate photo-electro-catalysts based on transition metal oxides, *Chem. Soc. Rev.* 42 (2013) 2401–2422.
- [12] A. Valdes, J. Brillet, M. Gratzel, H. Gudmundsdottir, H.A. Hansen, H. Jonsson, P. Klupfel, G.-J. Kroes, F. Le Formal, I.C. Man, Solar hydrogen production with semiconductor metal oxides: new directions in experiment and theory, *Phys. Chem. Chem. Phys. (PCCP)* 14 (2012) 49–70.

- [13] A. Fujishima, K. Honda, Electrochemical photolysis of water at a semiconductor electrode, *Nature* 238 (1972) 37–38.
- [14] F. Wang, C.D.V. Valentin, G. Pacchioni, Doping of WO<sub>3</sub> for photo-catalytic water splitting: hints from density functional theory, *J. Phys. Chem. C* 116 (2012) 8901–8909.
- [15] S. Wanga, H. Chena, G. Gaob, T. Butbreera, M. Lyua, S. Thaweesaka, J.-H. Yuna, A. Dub, G. Liuc, L. Wanga, Synergistic crystal facet engineering and structural control of WO<sub>3</sub> films exhibiting unprecedented photoelectrochemical performance, *Nano Energy* 24 (2016) 94–102.
- [16] Q. Mi, A. Zhanaidarova, B.S. Brunschwig, H.B. Gray, A quantitative assessment of the competition between water and anion oxidation at WO<sub>3</sub> photoanodes in acidic aqueous electrolytes, *Energy Environ. Sci.* 5 (2012) 5694–5700.
- [17] S.J. Yooa, S.U. Yunb, Y.-E. Sung, K.-S. Ahnc, Tungsten oxide bilayer electrodes for photoelectrochemical cells, *J. Power Sources* 195 (2010) 5422–5425.
- [18] G.-H. He, C.-J. Liang, Y.-D. Ou, D.-N. Liu, Y.-P. Fang, Y.-H. Xu, Preparation of novel Sb<sub>2</sub>O<sub>3</sub>/WO<sub>3</sub> photo-catalysts and their activities under visible light irradiation, *Mater. Res. Bull.* 48 (2013) 2244–2249.
- [19] K.H. Ng, L.J. Minggu, M.B. Kassim, Gallium-doped tungsten trioxide thin film photo-electrodes for photo-electrochemical water splitting, *Int. J. Hydrogen Energy* 38 (2013) 1–7.
- [20] L. Zhou, J. Zhu, M. Yu, X. Huang, Z. Li, Y. Wang, C. Yu, MoxW1-xO3·0.33H2O solid solutions with tunable band gaps, *J. Phys. Chem. C* 114 (2010) 20947–20954.
- [21] P. Liao, J.A. Keith, E.A. Carter, Water oxidation on pure and doped hematite (0001) surfaces: prediction of Co and Ni as effective dopants for electrocatalysis, *J. Am. Chem. Soc.* 134 (2012) 13296–13309.
- [22] O. Neufeld, M.C. Toroker, Platinum-Doped  $\alpha$ -Fe<sub>2</sub>O<sub>3</sub> for enhanced water splitting efficiency: a DFT+U study, *J. Phys. Chem. C* 119 (2015) 5836–5847.
- [23] G.A. d. Wijs, P.K. d. Boer, R.A. d. Groot, G. Kresse, Anomalous behavior of the semiconducting gap in WO<sub>3</sub> from first-principles calculations, *Phys. Rev. B* 59 (1999) 2684.
- [24] Y. Wu, M.K.Y. Chan, G. Ceder, Prediction of semiconductor band edge positions in aqueous environments from first principles, *Phys. Rev. B* 83 (2011) 235301.
- [25] Y. Ping, G. Galli, Optimizing the band edges of tungsten trioxide for water oxidation: a first-principles study, *J. Phys. Chem. C* 118 (2014) 6019–6028.
- [26] C.D. Valentin, F. Wang, G. Pacchioni, Tungsten oxide in catalysis and photo-catalysis: hints from DFT, *Top. Catal.* 56 (2013) 1404–1419.
- [27] Á. Valdés, G.J. Kroes, First principles study of the photo-oxidation of water on tungsten trioxide (WO<sub>3</sub>), *J. Chem. Phys.* 130 (2009) 114701–114709.
- [28] C. Zhu, C. Li, M. Zheng, J.-J. Delaunay, Plasma-Induced oxygen vacancies in ultrathin hematite nanoflakes promoting photoelectrochemical water oxidation, *ACS Appl. Mater Interfaces* 7 (2015) 22355–22363.
- [29] A. Hellman, B. Iandolo, B. Wickman, H. Grönbeck, J. Baltrusaitis, Electro-oxidation of water on hematite: effects of surface termination and oxygen vacancies investigated by first-principles, *Surf. Sci.* 640 (2015) 45–49.
- [30] X. Zhang, P. Klaver, R. van Santen, M.C.M. van de Sanden, A. Bieberle-Hütter, Oxygen evolution at hematite surfaces: the impact of structure and oxygen vacancies on lowering the overpotential, *J. Phys. Chem. C* 120 (2016) 18201–18208.
- [31] J. Rossmel, Z.W. Qu, H. Zhu, G.J. Kroes, J.K. Nørskov, Electrolysis of water on oxide surfaces, *J. Electroanal. Chem.* 607 (2007) 83–89.
- [32] M.T. Nguyen, S. Piccinin, N. Seriani, R. Gebauer, Photooxidation of water on defective Hematite (0001), *ACS Catal.* 5 (2015) 715–721.
- [33] M.C. Toroker, Theoretical insights into the mechanism of water oxidation on non-stoichiometric and titanium-doped Fe<sub>2</sub>O<sub>3</sub>(0001), *J. Phys. Chem. C* 118 (2014) 23162–23167.
- [34] X. Zhang, C. Cao, A. Bieberle-Hütter, Orientation sensitivity of oxygen evolution reaction on hematite, *J. Phys. Chem. C* 120 (2016) 28694–28700.
- [35] A. Hellman, B. Iandolo, B. Wickman, H. Grönbeck, J. Baltrusaitis, Electro-oxidation of water on hematite: effects of surface termination and oxygen vacancies investigated by first-principles, *Surf. Sci.* 640 (215) (2016) 45–49.
- [36] X. Zhang, C. Cao, A. Bieberle-Hütter, Enhanced electrochemical water oxidation: the impact of nanoclusters and nanocavities, *PCCP* 19 (2017) 31300–31305.
- [37] J. Hafner, Materials simulations using VASP – a quantum perspective to materials science, *Comput. Phys. Commun.* 177 (2007) 6–13.
- [38] G. Kresse, J. Hafner, Ab initio molecular dynamics for liquid metals, *Phys. Rev. B* 47 (93) (2016) 558–561.
- [39] G. Kresse, D. Joubert, From ultrasoft pseudopotentials to the projector augmented-Wave method, *Phys. Rev. B* 59 (1999) 1758–1775.
- [40] G. Kresse, J. Furthmüller, Efficient iterative schemes for ab initio total-energy calculations using a plane-wave basis, *Phys. Rev. B* 54 (1996) 11169–11186.
- [41] J.P. Perdew, K. Burke, M. Ernzerhof, Generalized gradient approximation made simple, *Phys. Rev. Lett.* 77 (1996) 3865–3868.
- [42] G. Kresse, D. Joubert, From ultrasoft pseudopotentials to the projector augmented-wave method, *Phys. Rev. B* 59 (1999) 1758–1775.
- [43] P.E. Blöchl, Projector augmented-wave method, *Phys. Rev. B* 50 (1994) 17953–17979.
- [44] C.F. Dickens, J.K. Nørskov, A theoretical investigation into the role of surface defects for oxygen evolution on RuO<sub>2</sub>, *J. Phys. Chem. C* 121 (2017) 18516–18524.
- [45] K.A. Stoerzinger, O. Diaz-Morales, M. Kolb, R.R. Rao, R. Frydendal, L. Qiao, X.R. Wang, N.B. Halck, J. Rossmel, H.A. Hansen, T. Vegge, I.E.L. Stephens, M.T.M. Koper, Y. Shao-Horn, Orientation-dependent oxygen evolution on RuO<sub>2</sub> without lattice exchange, *ACS Energy Lett.* 2 (2017) 876–881.
- [46] C. Santato, M. Ulmann, J. Augustynski, Photo electrochemical properties of nanostructured tungsten trioxide films, *J. Phys. Chem. B* 105 (2001) 936–940.
- [47] Á. Valdés, G.-J. Kroes, First principles study of the photo-oxidation of water on tungsten trioxide (WO<sub>3</sub>), *J. Chem. Phys.* 130 (2009) 114701.
- [48] N.B. Halck, V. Petrykin, P. Krtil, J. Rossmel, Beyond the volcano limitations in electrocatalysis – oxygen evolution reaction, *PCCP* 16 (2014) 13682–13688.
- [49] F. Wang, C. Di Valentin, G. Pacchioni, Doping of WO<sub>3</sub> for photocatalytic water splitting: hints from density functional theory, *J. Phys. Chem. C* 116 (2012) 8901–8909.
- [50] A. Hameed, M.A. Gondal, Z.H. Yamani, Effect of transition metal doping on photocatalytic activity of WO<sub>3</sub> for water splitting under laser illumination: role of 3d-orbitals, *Catal. Commun.* 5 (2004) 715–719.